Supplemental Material for "Charge-Induced Phase Transition in Encapsulated $HfTe_2$ Nanoribbons"

Derek Popple[1-4], Mehmet Dogan[2,3], Tony Vo Hoang[2], Scott Stonemeyer[1-4], Peter Ercius[5], Karen C. Bustillo[5], Marvin Cohen[2,3], Alex Zettl[2-4,*]

1. Department of Chemistry, University of California Berkeley, Berkeley, CA 94720
2. Department of Physics, University of California Berkeley, Berkeley, CA 94720
3. Materials Sciences Division, Lawrence Berkeley National Lab, 1 Cyclotron Road, Berkeley CA, 94720
4. Kavli Energy NanoScience Institute at the University of California at Berkeley and the Lawrence Berkeley National Laboratory, Berkeley, CA, 94720
5. National Center for Electron Microscopy, Molecular Foundry, Lawrence Berkeley National Lab, 1 Cyclotron Road, Berkeley CA, 94720

Synthesis of $HfTe_2$@CNT

$HfTe_2$ nanoribbons were synthesized using similar procedure to that outlined previously for $NbTe_3$, VTe_3 and $NbSe_3$ by the Zettl Group. [1,2]. Carbon nanotubes (CheapTubes, nominally advertized as 90% SW-DW CNTs, but containing many larger diameter, multi-walled tubes) were oxidized in air for 15 minutes to remove end caps. Stoichiometric amounts of powdered Hf and Te shot were added into a quartz ampoule containing end opened carbon nanotubes and 5 mg/cm^3 of I_2 and sealed under vacuum. The ampoule was heated rapidly to 900 °C for 72 hours and then cooled to room temperature over 72 hours. The ampoule contents were sonicated in pure IPA for 30 minutes to prevent aggregation before dropcasting the suspension onto a copper/lacey C TEM grid (Ted Pella). Nanotubes that became successfully filled with $HfTe_2$ nanoribbons typically had wall number between two and four, with inner diameters ranging from 1.3 to 7.4 nm.

Electron microscopy

Initial imaging to confirm filling of encapsulated nanoribbons was performed on a JEOL 2010 operated at 80kV. Atomic-resolution STEM imaging to characterize the structure and phase of the nanoribbons was completed at the National Center for Electron Microscopy on TEAM 0.5, a Titan 80-300 with an ultra-twin pole piece gap and DCOR probe aberration corrector. The scope was operated at 80 kV and a semi-convergence angle of 30 mrad. Images were acquired using the HAADF-STEM detector with an inner angle of 60 mrad and a beam current of approximately 70 pA. Spectrum-imaging using energy dispersive x-ray spectroscopy was acquired at the National Center for Electron Microscopy on a FEI TitanX at 300kV. The electron beam current was ~350pA; the dwell time was 28us at each 0.3 nm pixel for an accumulated 214 frames.

STEM images were acquired before and after the EDS mapping in order to confirm that no visible beam damage was evident. Custom energy ranges were defined in order to avoid overlap from I (L_α ~3.9keV) used in the synthesis and Cu (K_α ~8.0keV) from the TEM grid. Region F1 corresponds to the counts related to the Hf $L_{\beta 2}$ transition. F1 is centered at 9.339 keV and has a width of 0.134 keV. Region F2 was used for quantification of the Te $L_{\alpha 1}$ transition. F2 is centered at 3.786 keV and has a width of 0.129 keV.

STEM simulations were performed using the Prismatic software version 2.0 using the multislice algorithm with GPU acceleration. [3] The sample potential pixel size was 0.045 Angstroms and a slice thickness of 1 Angstrom was used. The microscope parameters were 80 kV accelerating voltage, 30 mrad convergence semi-angle, HAADF detector angles of 46 to 241 mrad (inner to outer, respectively), and real space probe step size of 0.2 Angstroms. 20 frozen phonon configurations were incoherently summed.

Computational Details

We based our calculations on density functional theory (DFT) in the Perdew–Burke–Ernzerhof generalized gradient approximation (PBE GGA). [4] Using the plane-wave based QUANTUM ESPRESSO software package, [5] we relaxed atomic configurations and electronic structures. Norm-conserving pseudopotentials with a 80 Ry plane-wave energy cutoff were used. [6] We included van der Waals interactions by employing the semi-emprical DFT-D3 method. [7] We used a 12×12 Monkhorst–Pack k-point mesh to sample the Brillouin zone for 1×1 unit-cell calculations, and adjusted the k-point mesh accordingly in the supercell cases. [8] Because we used periodic boundary conditions, we separated between periodic copies by a distance of ~16 Å

to eliminate unphysical interactions. Coordinates of all the atoms were relaxed until the forces fell below 10^{-5} Ry/a_0 in all three Cartesian directions (a_0: Bohr radius). For calculations of nanoribbons encapsulated by nanotubes, which included much larger numbers of atoms (in the 100s), we used the atomic orbital based SIESTA package. [9] To study transition states, we employed the nudged elastic band (NEB) method with climbing images, as implemented in QUANTUM ESPRESSO. [10,11] In cases where the hybrid functional by Heyd–Scuseria–Ernzerhof (HSE06) was used, a 6×6 Fock grid was employed. [12]

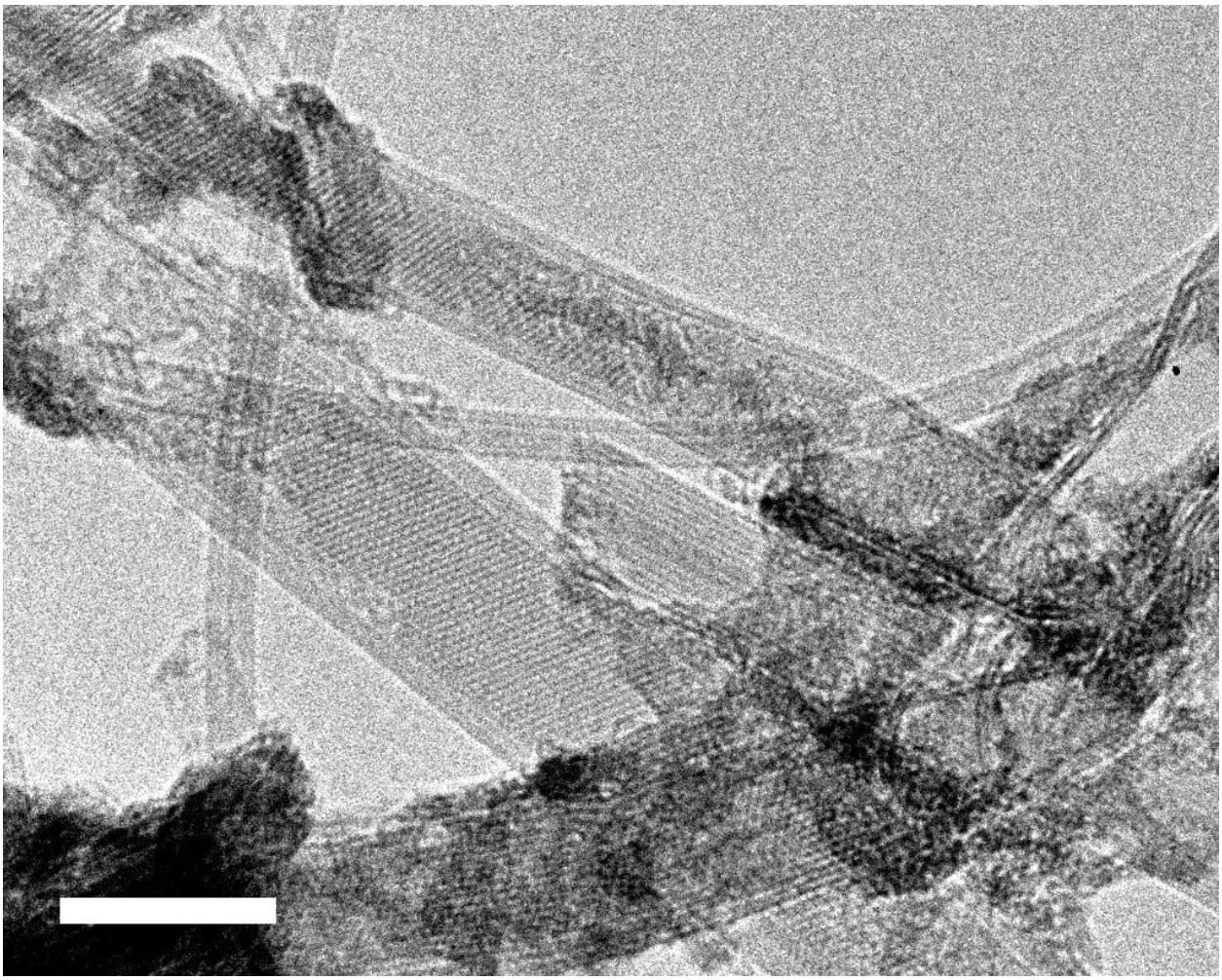

Figure S1. TEM of $HfTe_2$@CNT nanoribbons. In the bright field TEM image several nanoribbons and the walls of the encapsulating nanotubes are observed. The encapsulating nanotubes are double and triple walled with respective inner diameters of 4.1 and 7.3 nm. Scalebar: 10 nm.

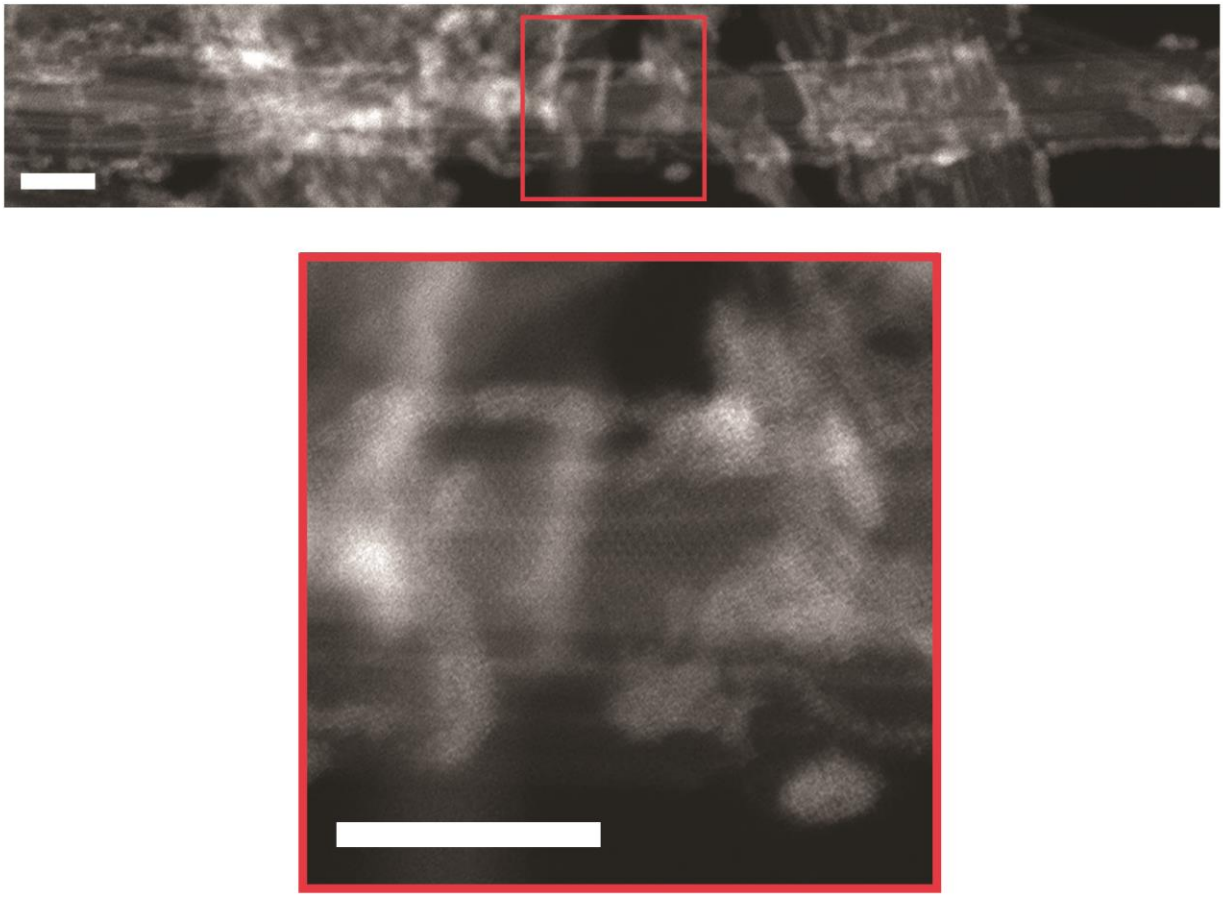

Figure S2. Length of nanoribbon filling. A pair of nanoribbons show continuous filling longer than 100 nm. A higher magnification image of the same region (indicated with a red box) shows the 1H lattice in both ribbons. Scalebar: 10 nm.

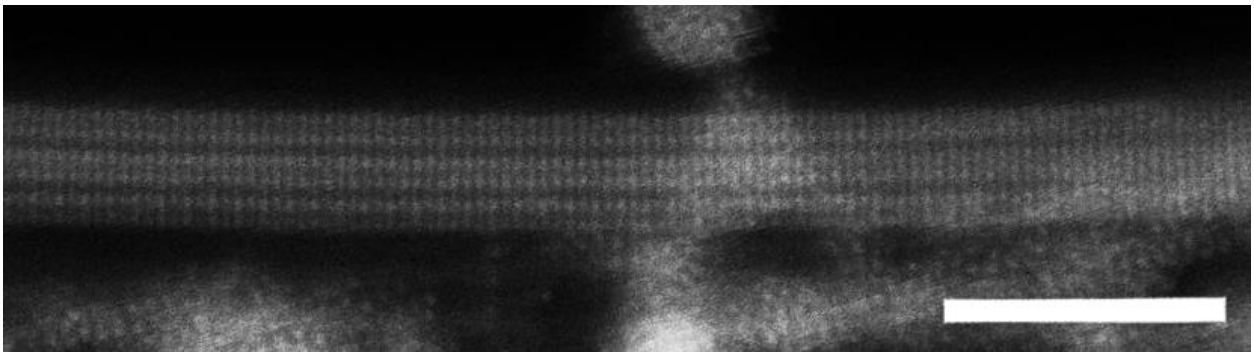

Figure S3. HAADF-STEM image of edge-on view of nanoribbon. In this nanotube, a trilayer of $HfTe_2$ is viewed edge-on showing the expected sandwich structure of a TMD. Note that the interlayer spacing is ~0.6nm. Encapsulating nanotube is a double-walled CNT with a measured inner diameter of 2.2 nm. Scalebar: 5 nm.

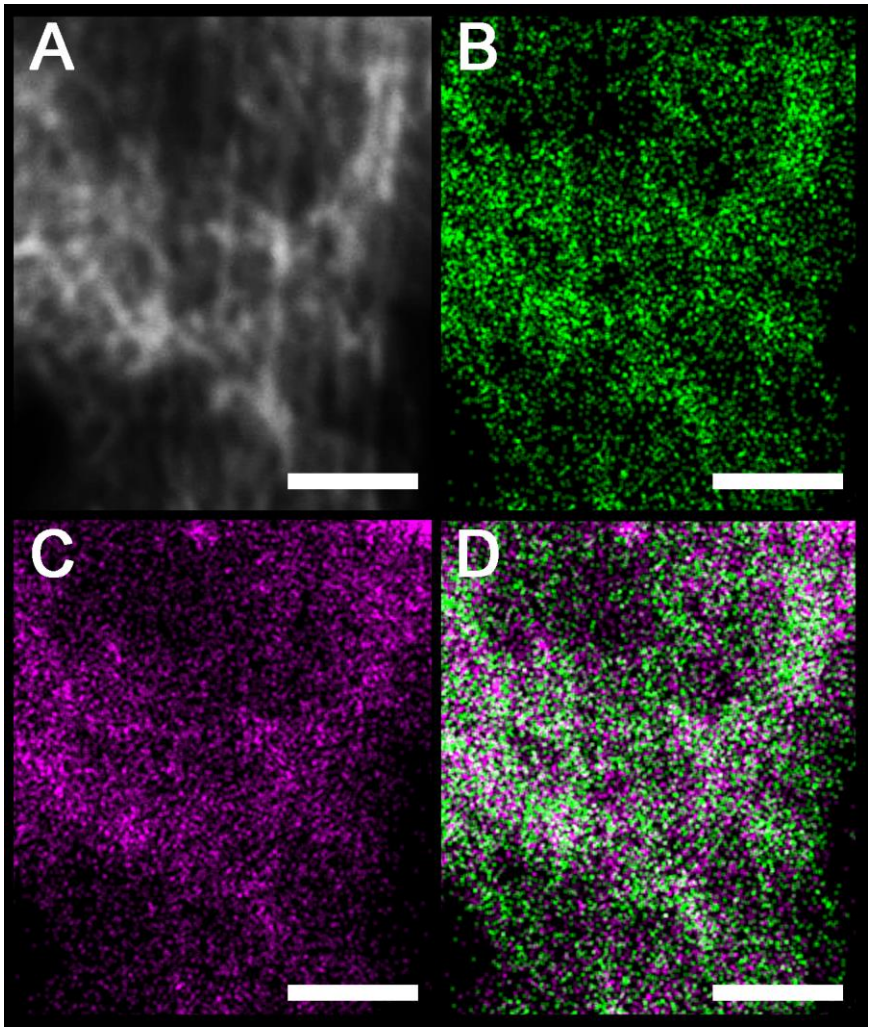

Figure S4. Elemental analysis of bundle of $HfTe_2$@CNT. EDX was conducted on the region shown in the HAADF-STEM image (A). Elemental maps are created showing the presence of Hf ($L_{\beta 2}$) in green (B) and Te ($L_{\alpha 1}$) in magenta (C). A stacked map (D) shows white spots where the Hf and Te overlap. Scalebar: 50 nm.

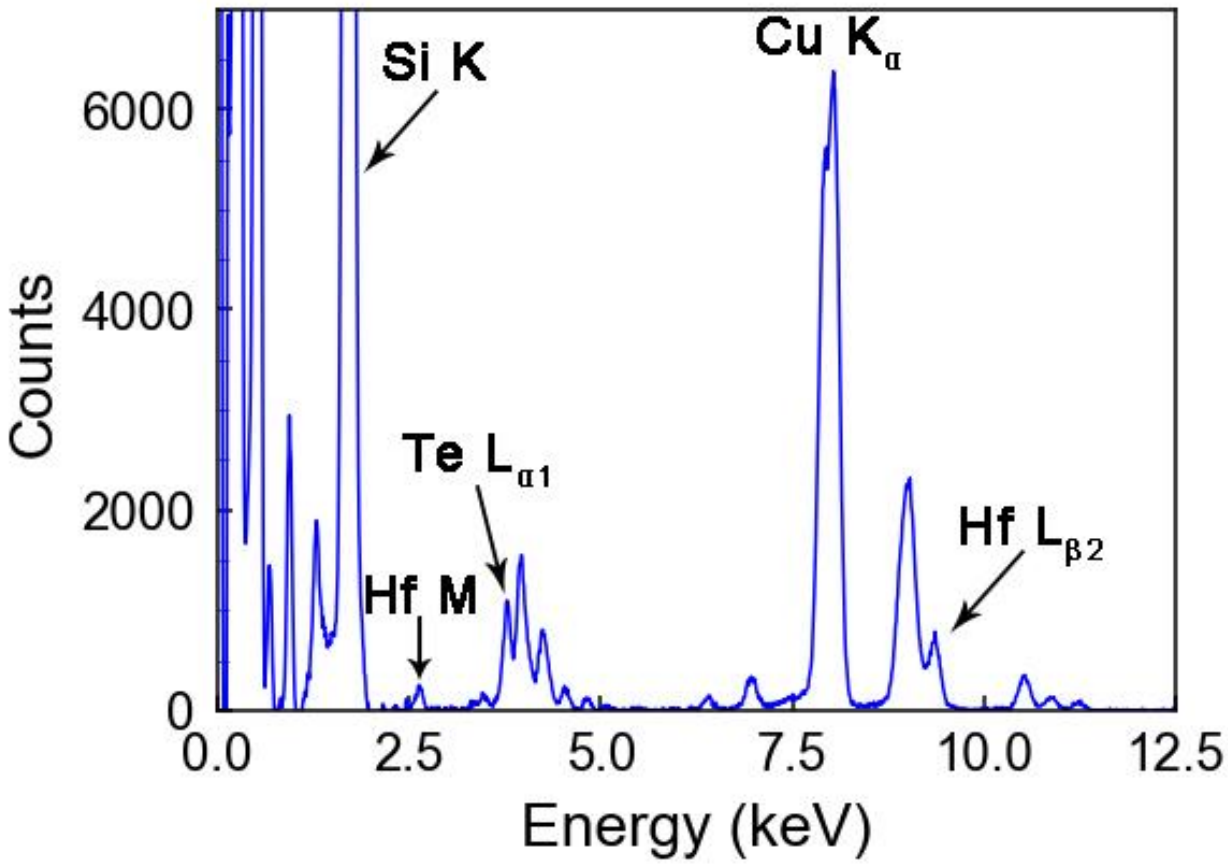

Figure S5. EDS spectrum of $HfTe_2$@CNT. EDS spectrum of a bundle of nanotubes filled with $HfTe_2$. The presence of a large peak from copper is attributed to the copper/lacey carbon TEM grid.

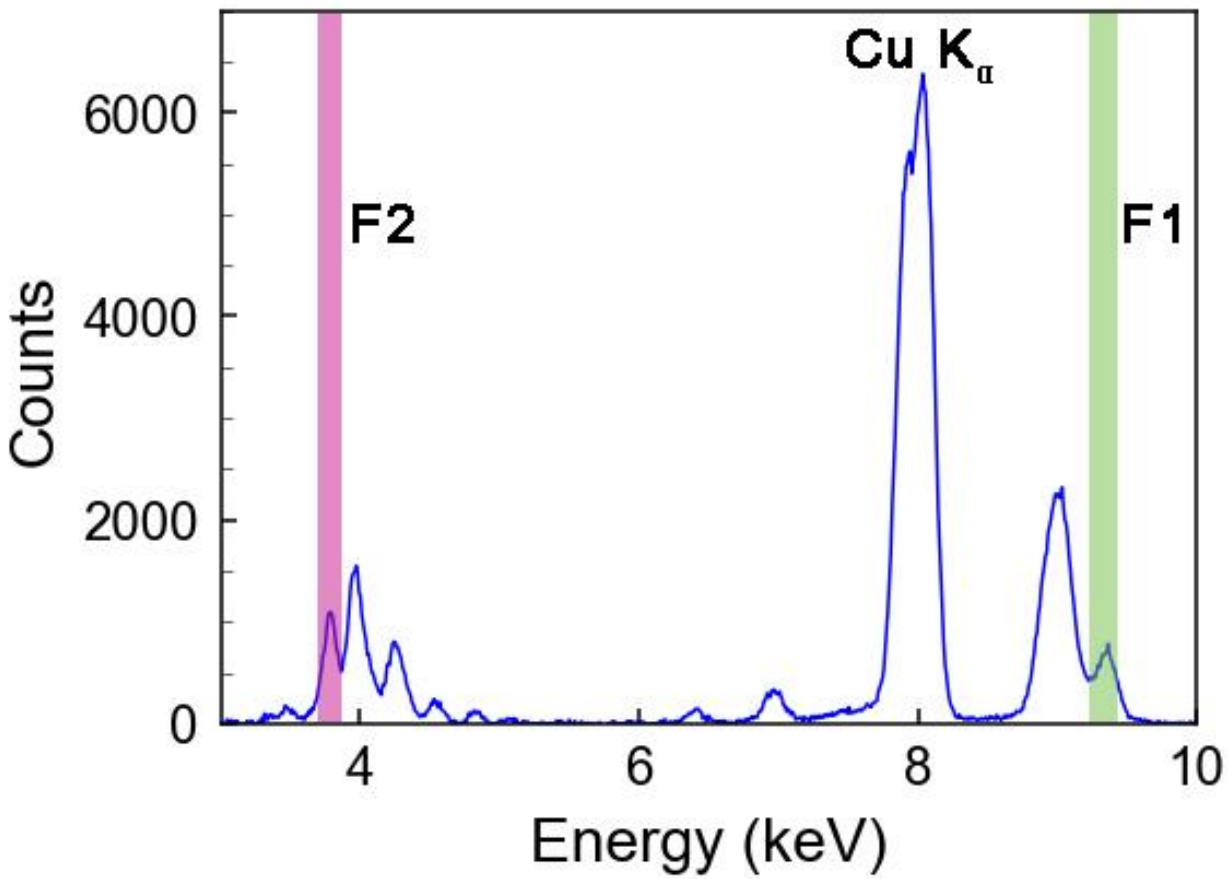

Figure S6. Region of interest for EDS spectrum of $HfTe_2$@CNT. Area of spectrum between 3-10 keV was used to define custom energy regions for elemental mapping of Hf and Te in Figure S4. Custom energy ranges were used for mapping to avoid overlap of signal from other elements in the sample. Energy region F1 was used to quantify the counts related to the Hf $L_{\beta 2}$ transition. F1 is centered at 9.339 keV and has a width of 0.134 keV. Energy region F2 was used for quantification of the Te $L_{\alpha 1}$ transition. F2 is centered at 3.786 keV and has a width of 0.129 keV. Fe at 6.4keV and Co at 6.9keV are from the TEM column.

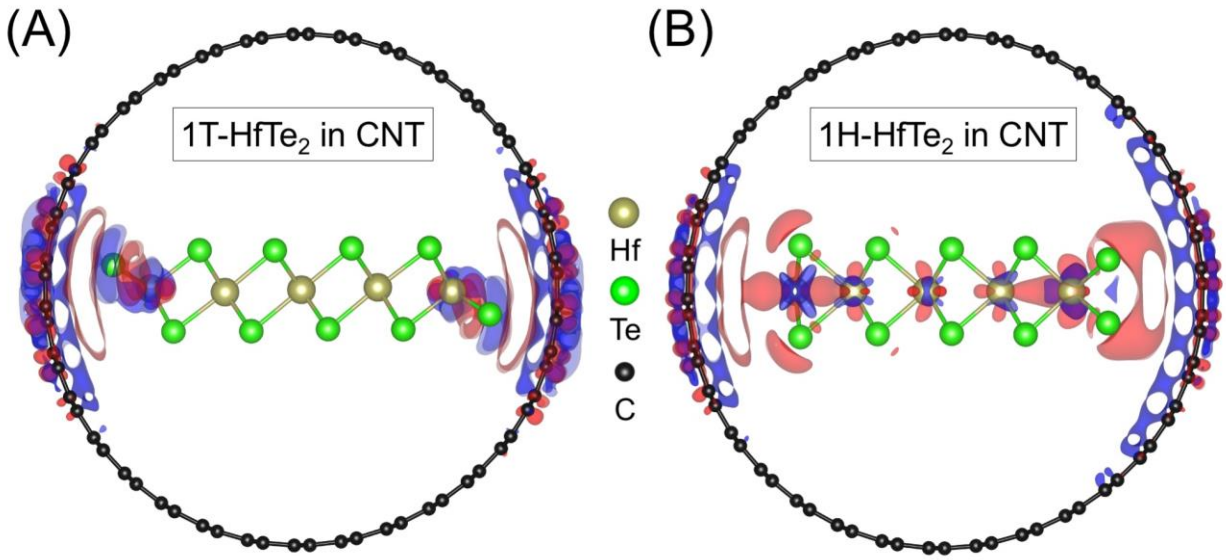

Figure S7. Charge transfer in the encapsulated nanoribbons. Spatial visualization of the electron transfer between the carbon nanotube and $HfTe_2$ nanoribbon. (A) 1T NR and (B) 1H NR. In both cases, the width of the NR is 5 u.c. Positive and negative values of electron transfer correspond to blue and red isosurfaces, respectively.

Movie S1. STEM movie showing ribbon dynamics. In the movie, a nanoribbon undergoes a phase change from the 1T phase to 1H, and then back to 1T. The region where the phase change is most visible is highlighted with a red box. Image acquired with a dwell time of 3 μs (0.94 s per frame).

References

[1] T. Pham, S. Oh, P. Stetz, S. Onishi, C. Kisielowski, M. L. Cohen, and A. Zettl, *Torsional Instability in the Single-Chain Limit of a Transition Metal Trichalcogenide*, Science **361**, 263 (2018).

[2] S. Stonemeyer, J. D. Cain, S. Oh, A. Azizi, M. Elasha, M. Thiel, C. Song, P. Ercius, M. L. Cohen, and A. Zettl, *Stabilization of $NbTe_3$, VTe_3, and $TiTe_3$ via Nanotube Encapsulation*, J. Am. Chem. Soc. **143**, 4563 (2021).

[3] L. Rangel DaCosta, H. G. Brown, P. M. Pelz, A. Rakowski, N. Barber, P. O'Donovan, P. McBean, L. Jones, J. Ciston, M. C. Scott, et al., *Prismatic 2.0 – Simulation Software for Scanning and High Resolution Transmission Electron Microscopy (STEM and HRTEM)*, Micron **151**, 103141 (2021).

[4] J. P. Perdew and A. Zunger, *Self-Interaction Correction to Density-Functional Approximations for Many-Electron Systems*, Physical Review B **23**, 5048 (1981).

[5] P. Giannozzi, S. Baroni, N. Bonini, M. Calandra, R. Car, C. Cavazzoni, D. Ceresoli, G. L. Chiarotti, M. Cococcioni, I. Dabo, et al., *QUANTUM ESPRESSO: A Modular and Open-Source Software Project for Quantum Simulations of Materials*, Journal of Physics: Condensed Matter **21**, 395502 (2009).

[6] D. R. Hamann, *Optimized Norm-Conserving Vanderbilt Pseudopotentials*, Physical Review B **88**, 085117 (2013).

[7] S. Grimme, J. Antony, S. Ehrlich, and H. Krieg, *A Consistent and Accurate Ab Initio Parametrization of Density Functional Dispersion Correction (DFT-D) for the 94 Elements H-Pu*, The Journal of Chemical Physics **132**, 154104 (2010).

[8] M. L. Cohen, M. Schlüter, J. R. Chelikowsky, and S. G. Louie, *Self-Consistent Pseudopotential Method for Localized Configurations: Molecules*, Physical Review B **12**, 5575 (1975).

[9] J. M. Soler, E. Artacho, J. D. Gale, A. García, J. Junquera, P. Ordejón, and D. Sánchez-Portal, *The SIESTA Method for Ab Initio Order-N Materials Simulation*, J. Phys.: Condens. Matter **14**, 2745 (2002).

[10] G. Henkelman, G. Johannesson, and H. Jonson, *Methods for Finding Saddle Points and Minimum Energy Paths*, in *Theoretical Methods in Condensed Matter Chemistry* (2000).

[11] G. Henkelman, B. P. Uberuaga, and H. Jónsson, *A Climbing Image Nudged Elastic Band Method for Finding Saddle Points and Minimum Energy Paths*, The Journal of Chemical Physics **113**, 9901 (2000).

[12] J. Heyd, G. E. Scuseria, and M. Ernzerhof, *Hybrid Functionals Based on a Screened Coulomb Potential*, J. Chem. Phys. **118**, 8207 (2003).